PROCEEDINGS of the
23rd International Congress on Acoustics
9 to 13 September 2019 in Aachen, Germany

Simulation of flow noise generated by the interaction of inflow turbulence with the leading edge of a foil

Mattias LIEFVENDAHL[(1)]

[(1)]Swedish Defence Research Agency (FOI), Sweden, mattias.liefvendahl@foi.se

Abstract

Noise generated by the interaction of inflow turbulence with a lifting surface may be of interest for a number of hydrodynamic applications, including a propeller operating in non-cavitating condition. In the present work, simulation-based methods are applied for the prediction of the radiated noise from a wing in strong inflow turbulence, at a chord-based Reynolds number, $\mathrm{Re}_c = 256\,000$, and a Mach number of 0.09. The case has also been investigated experimentally, and a comparison is made between measurement and simulation results. Large-eddy simulation is employed to predict the flow, with synthetic turbulence fluctuations applied at the inflow boundary. The LES-results are then used to compute the acoustic source terms of an acoustic analogy. The sensitivity of the results to inflow turbulence level and turbulent length scale is investigated. The analysis is focused on the unsteady flow features associated with flow noise generation.

Keywords: Large-eddy simulation, Flow noise, Hydroacoustics

1 INTRODUCTION

Flow noise generated by a lifting surface is an important model problem for a number of hydrodynamic applications, including a propeller operating in non-cavitating condition. For a lifting surface, several flow mechanisms may induce significant flow-generated sound, including the trailing edge flow, the tip vortex and the interaction between inflow turbulence and the leading edge, [2]. In certain conditions, including strong inflow turbulence, the leading edge contribution may be dominant. In the present study, such a test case is investigated, primarily by simulation-based methods.

Pioneering studies of leadinge-edge noise was carried out in the 1970:ies. Amiet derived an analytical model of the radiated sound from a thin foil, [1], by analysis of scattering from a semi-infinite plane. See [13] for a later review of developments and refinements of this approach which is widely used. An aeroacoustic measurement campaign of leadinge-edge noise in an open jet anechoic wind tunnel, [11], was made in connection with these original investigations. This type of models require a characterization of the inflow turbulence in terms of intensity, in particular of the fluctuations in the upwash velocity component, and various length scales associated with the turbulence.

The development of computational technology has lead to the possibility of employing CFD, in particular scale-resolving simulations, in order to directly simulate the flow mechanisms generating sound. Such is the approach of the present paper, where LES is employed to simulate the flow around the foil, including the inflow turbulence which was generated by a synthetic method, [7]. The use of such high-fidelity methods has the potential to improve predictions as compared to classical techniques, e.g. concerning the effect of wing thickness and the deformation of turbulence in the flow around the wing. This LES approach, and its use to compute sound sources in an acoustic analogy, was applied in, [9], to investigate aeolian tones.

The simulated case consists of isotropic and homogeneous turbulence impinging on a wing with a NACA-0012 profile at zero angle of attack. Both radiated sound and the inflow turbulence has been investigated experimentally for this case, [15]. The flow is simulated at conditions corresponding to the experimental set-up, and the results are analyzed with a particular focus on to flow around the leading edge with a view to sound generation. Furthermore, the influence of intensity and length scale of the incoming turbulence is investigated.

1.1 Case description

The main physical parameters of the simulated case are given in table 1, and the relatively thick wing profile is shown in figure 1. The turbulence characteristics have been inferred from the results reported in [15]. The inflow turbulence of the simulations is characterized by a turbulence intensity, $k = 4.86\,\mathrm{m}^2/\mathrm{s}^2$, and a turbulent length scale of, $l_t = 15\,\mathrm{mm}$, which are input parameters to the synthetic turbulence generation method.

Table 1. Main physical parameters, corresponding to the experimental measurements, [15], leading to a Mach-number, $\mathrm{Ma} = V_0/c = 0.09$, and a chord-based Reynolds-number, $\mathrm{Re}_c = cV_0/\nu = 256\,000$.

Quantity	Notation	Value	Unit
Wing length	L	0.2	m
Wing chord	c	0.1	m
Max. wing thickness	t	11.9	mm
Velocity	V_0	30	m/s
Kin.visc.	ν	$1.17{\cdot}10^{-5}$	m^2/s
Sound speed	c_0	333	m/s

Figure 1. The NACA-0012 wing profile.

The simulation campaign, see table 2, is designed to investigate the sensitivity of the flow and the radiated sound to changes in turbulence intensity and length scale. The first set of four simulations (Case 1–4) tests independent variation of k and l_t. The second set of three simulations (Case 5–7) tests variation of the turbulent length scale l_t around the value measured in [15]. The simulated time intervals are described in section 2, in connection with a description of time step size and other numerical parameters.

Table 2. Simulation campaign. Turbulent kinetic energy, k, and turbulent length scale, l_t, is varied between simulation cases. For the remaining physical parameters, see table 1.

Case	1	2	3	4	5	6	7
k ($\mathrm{m}^2/\mathrm{s}^2$)	1.50	1.50	3.00	3.00	4.86	4.86	4.86
l_y (mm)	10	15	10	15	10	15	20

Throughout this paper, the following two coordinate systems are used. A Cartesian coordinate system with the x-axis pointing in the main flow direction, with, $x = 0$, at the wing leading edge, the y-axis in the spanwise direction, with, $y = 0$, at mid-span, and the z-axis in order to have a right-handed coordinate system, with, $z = 0$, in the plane of the wing. A polar coordinate system in the xz–plane, with radial coordinate, $r = (x^2 + z^2)^{1/2}$, and the polar coordinate defined with, $\theta = 0$, in the upstream direction.

2 METHODS

The computational approach consists of incompressible LES of the flow around the foil, and then the application of an acoustic analogy for the far-field radiated sound. The source terms in the acoustic analogy are approximated using the simulated flow. Spatial filtering of the incompressible and viscous momentum equation

of the flow leads to the following equation, see [14].

$$\frac{\partial \overline{v}_i}{\partial t} + \overline{v}_j \frac{\partial \overline{v}_i}{\partial x_j} = -\frac{1}{\rho_0}\frac{\partial \overline{p}}{\partial x_i} + \nu \frac{\partial^2 \overline{v}_i}{\partial x_j x_j} - \frac{\partial \tau_{ij}}{\partial x_i x_j}$$

Here, $\tau_{ij} = \overline{u_i u_j} - \overline{v}_i \overline{v}_j$, is the subgrid stress tensor and overbar indicated filtered quantities. LES subgrid modelling consists of providing a computable expression for τ_{ij}. In the simulations of this paper, an implicit LES approach was used, where the subgrid dissipation is considered to be represented by the numerical diffusion, see e.g. [6]. See, [14], for a general reference on LES and, [9], and the references therein for more information about the particular approach and implementation used here. From now on, the overbar notation is dropped and use is made of the notation, $u = v_1$, $v = v_2$, and $w = v_3$ for the velocity components. The acoustic analogy employed was proposed in, [5], and also employed in [8, 9]. The formulation supports so-called porous acoustic surfaces for the sampling of flow quantities for source computation, but here the acoustic surface is chosen to coincide with the foil, which reduces the method to that proposed by Curle, [3]. The results analysis below is however strongly focused on the flow around the leading edge.

The flow solver and the acoustic analogy have been implemented in the open source software library OpenFOAM, see [10] and the references therein. The finite volume method was used to discretize the LES equations, with cell-centered storage of the unknown quantities. All approximations are second-order accuracte. For the convective scheme, a blending is used with 25% second-order upwind and 75% linear scheme. This ensures an adequate level of numerical dissipation for ILES, [12]. The computational domain is the following rectangular block.

$$-24\,\text{cm} < x < 110\,\text{cm} \qquad -10\,\text{cm} < y < 10\,\text{cm} \qquad -50\,\text{cm} < z < 50\,\text{cm}$$

Recall that the wing chord is, $c = 10\,\text{cm}$, and the leading edge is located at, $(x,z) = (0,0)$. At the inflow, $x = -24\,\text{cm}$, a uniform inflow, with turbulence characterized by k and l_t, is prescribed. This boundary condition for synthetic turbulence, [7], is implemented in an openly available library to OpenFOAM.

The computational grid is generated as a block-structured grid with hexahedral cells. Care must be taken to make the grid sufficiently fine to sustain the convection of the inflow turbulence and also to allow a proper representation of the boundary layer over the wing. The total number of cells in the grid is $46 \cdot 10^6$. Between the inflow and the leading edge, the cells are roughly rectangular blocks with maximum cell edge length in the three coordinate directions of, $\Delta x \approx 1.0\,\text{mm}$, $\Delta y \approx 1.0\,\text{mm}$, and $\Delta z \approx 0.5\,\text{mm}$. This is to be compared with the simulated turbulent length scales, $10\,\text{mm} < l_t < 20\,\text{mm}$. The Re-number is sufficiently low so that there is no transition to turbulence in the boundary layer over the wing. Hence the wing is simulated as laminar and no wall model is employed. This implies that very thin cells (aiming for $y^+ \approx 1$) must be used adjacent to the wing in order to resolve the boundary layer profile. The typical height of the first cell layer over the wing is, $\Delta h \approx 10\,\mu\text{m}$.

The simulations are time-resolved and CFL-number limited. The time step, $\Delta t = 1\,\mu\text{s}$, was used in all simulations. This time step can be compared to the wing flow-pass time, $T_{fp} = c/V_0 \approx 3.33\,ms$. The simulations were started from a uniform flow state and simulated during 20 ms ($= 6T_{fp}$) before the flow was considered to have assumed a statistical steady state. After that, flow statistics was gathered during at least 10 ms for all simulation cases, and up to 90 ms for the most interesting cases.

3 RESULTS

An illustration of the simulated flow around the wing, for Case 6, is shown in figure 2. From the stagnation line along the leading edge, the flow is accelerated over the wing until it reaches the adverse pressure gradient near the trailing edge. The scales of the inflow turbulent structures, $l_t = 15\,\text{mm}$, can be seen relative to the wing thickness, $t = 11.9\,\text{mm}$. The radius of curvature at the leading edge is, $r_c = 1.6\,\text{mm}$. Additional unsteadiness develops in the flow near the trailing edge, as can be seen in the surface pressure distribution. The structure of the turbulence in the near wake of the wing can also be seen in the figure.

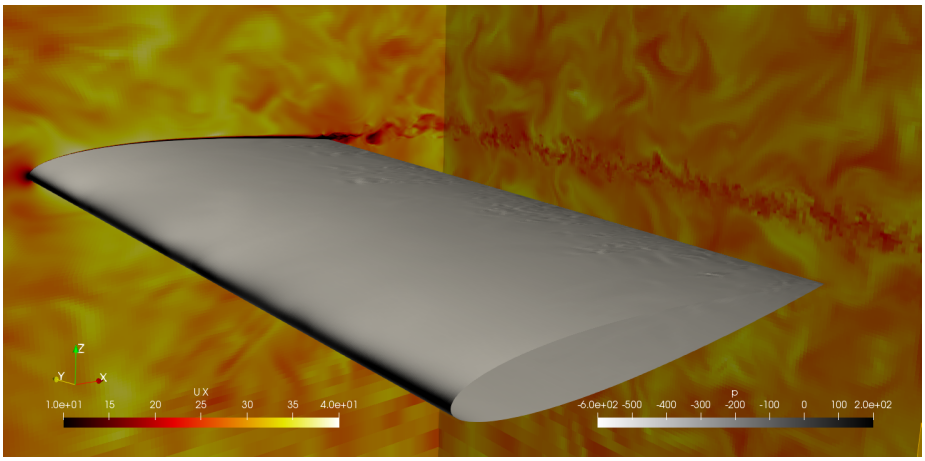

Figure 2. Illustration of the simulated flow around the wing (Case 6). The instantaneous axial velocity, u, is shown on a streamwise plane (y constant) and on a cross-plane (x constant) in the near wake. The range of the color scale is, $10 m/s < u < 40 m/s$. The instantaneous pressure distribution on the wing is shown in grey scale with range, $-600\,\text{Pa} < p < 200\,\text{Pa}$.

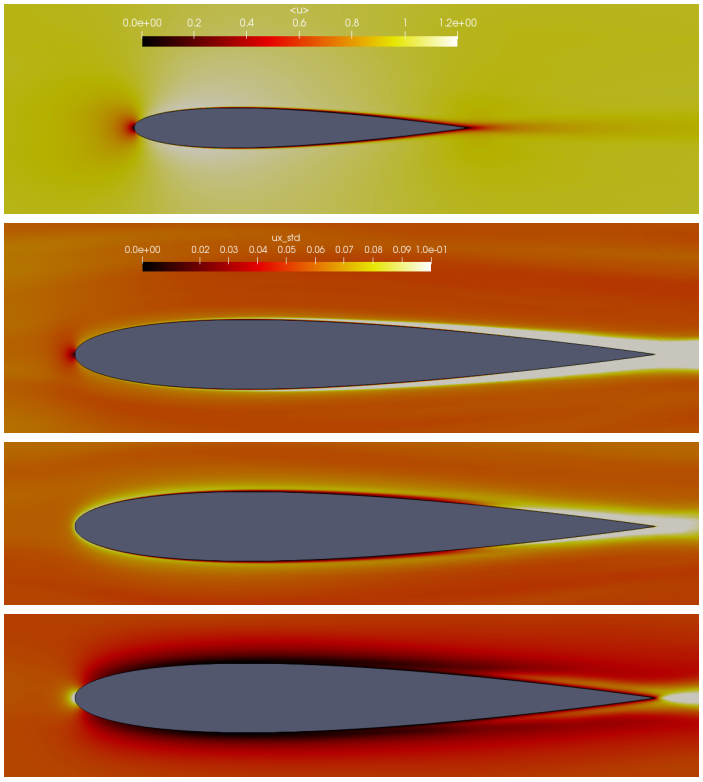

Figure 3. Flow statistics for Case 6. The normalized mean axial velocity, $\langle u \rangle / V_0$, is shown in the top graph, with color scale in the range, 0.0 – 1.2. The second graph shows the standard deviation of axial velocity fluctuations, normalized by the free-stream velocity, $\sigma(u')/V_0$, with color scale in the range, 0 – 10%. The third graph shows, $\sigma(v')/V_0$, and the bottom graph shows, $\sigma(w')/V_0$, both with the same color scale range, 0 – 10%.

The flow statistics, for Case 6, is shown in figure 3. The mean flow is not significantly affected by the strong inflow turbulence, but shows the usual behaviour for a wing at no angle of attack. Near the leading edge, the level of fluctuations behaves quite differently for the three components of velocity. The inflow value, $k = 4.86\,\mathrm{m}^2/\mathrm{s}^2$, corresponds to, $\sigma(u')/V_0 = 6\%$, and the same for the other two velocity components. This level is roughly maintained as the inflow turbulence is convected from the inflow to the leading edge. In the vicinity of the leading edge, the axial fluctuations, $\sigma(u')$, decreases sharply while the upwash fluctuations, $\sigma(w')$, displays a rapid increase. The spanwise fluctuations, $\sigma(v')$, exhibits a mild increase near the whole wing surface, including at the leading edge.

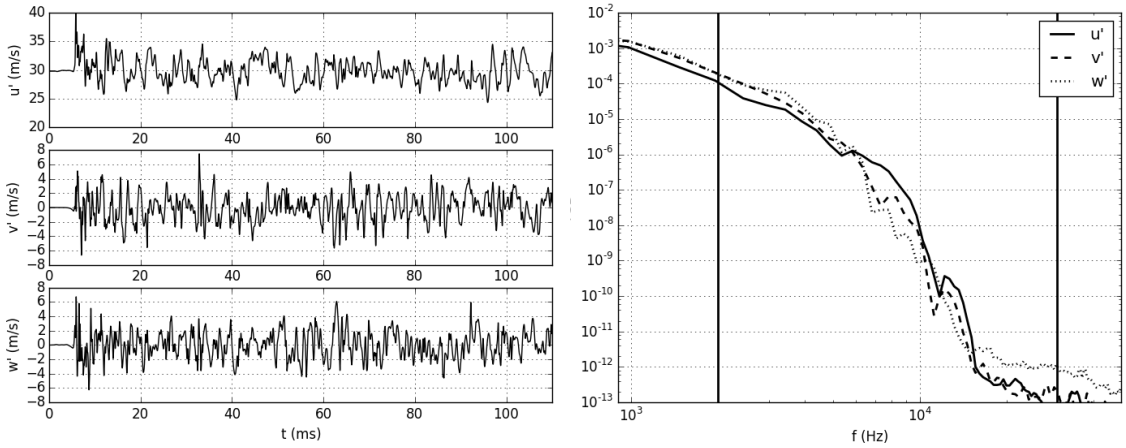

Figure 4. Time series and spectrum of velocity components in a point 10 cm upstream of the leading edge, at $(y,z) = 0,0$, for Case 6. The left graph shows the time series of the three velocity components during the complete simulation interval. The right graph shows the power spectral density of the corresponding time series. The vertical lines in the right graph indicates the turbulence frequency, $f_t = 2\,\mathrm{kHz}$, and the grid frequency, $f_{\Delta x} = 30\,\mathrm{kHz}$.

The inflow turbulence, for Case 6, is shown in figure 4, in terms of the velocity signals (both time series and spectrum) in the indicated point location 10 cm upstream of the leading edge. The initial flat part in the time series, up to $t \approx 5\,\mathrm{ms}$, indicates the time it takes for the inflow turbulence to be convected from the inflow boundary to the point. After that, the curves show similar level of turbulent fluctuations around the local mean value. The influence of the wing is negligible at this point. The power spectral densities of the velocity fluctuations are also shown in figure 4. The length scale of the inflow turbulence, $l_t = 15\,\mathrm{mm}$, which is convected with the free-stream velocity, corresponds to a frequency, $f_t = V_0/l_t = 2\,\mathrm{kHz}$, which is indicated in the graph. Also of interest are the finest scales which are possible to resolve in the LES computation. To get an idea of this, the grid size, $\Delta x \approx 1.0\,\mathrm{mm}$, can likewise be converted to a frequency, $f_{\Delta x} = V_0/\Delta x \approx 30\,\mathrm{kHz}$, which is also indicated in the graph. The power spectral densities decrease with a factor $\sim 10^9$ between these two frequencies.

The turbulence deformation around the wing was shown in figure 3. In figure 5, the same quantities are plotted along a streamwise line upstream of the leading edge of the wing. Figure 5 also compares results from Cases 5–7 and measurement data from [15]. The focus is on the levels of fluctuations, but the mean velocity curve is included to show the upstream influence of the leading edge, which is noticeable up to $\approx 5\,\mathrm{mm}$ upstream of the leading edge. The level of fluctuations in the velocity components show very significant discrepancies between the simulations and the measurements. The measurement data is taken from figure 12b in [15]. It should be pointed out that this is a difficult aspect of the flow to measure, and also to simulate to some extent. First it is observed that there is a problem with the measurement data for $\sigma(u')$, since this quantity is required to decay

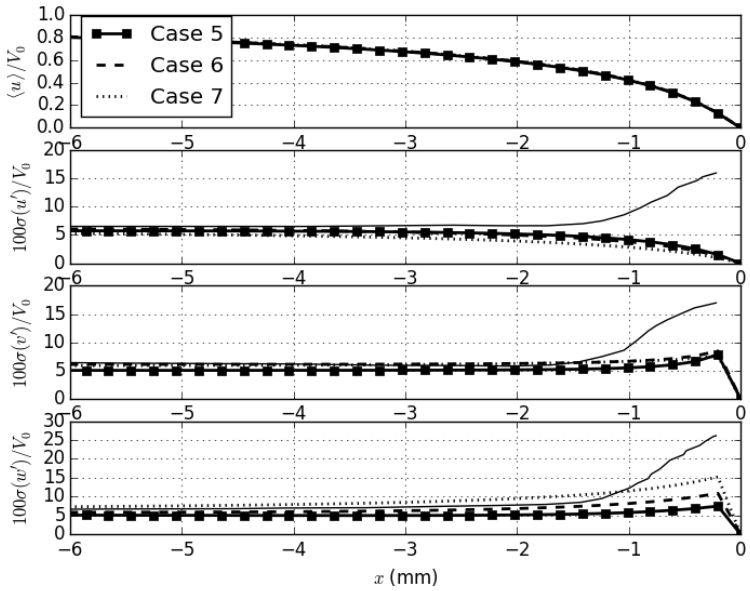

Figure 5. Flow statistics along a streamwise line at, $(y,z) = (0,0)$, upstream of the wing leading edge. Comparison of results from Case 5–7 (line style indicated in the figure) with measurements from figure 12b in [15], shown with the full line in the three graphs (for fluctuation levels). The top graph (contains no measurement data) shows the normalized axial mean velocity, $\langle u \rangle / V_0$. The remaining three graphs show the standard deviation of the velocity fluctuations in percent, for u', v' and w' respectively.

to zero at the leading edge. As is clear from figure 3, only a small deviation in the measurement point implies that this decay is missed. For the other two components, spanwise (v') and upwash (w'), both simulations and measurements show a significant increase close to the leading edge, at a distance of less than 2 mm, say. The measured increase is however very much larger than that predicted by simulations. E.g. $\sigma(v')$ increases from the inflow value of 6% to 17% in the measurements, whereas the maximum value in the simulations of this quantity is only around 9%. Similar discrepancy is also noted for $\sigma(w')$. Based on the simulation results, the effect of turbulent length scale can also be investigated. The only quantity in figure 5 which is affected by this is the upwash fluctuations, $\sigma(w')$. An increase in turbulent length scale leads to an increase in peak $\sigma(w')$. The maximum for Case 5 ($l_t = 10$ mm) is 8%, the maximum for Case 6 ($l_t = 15$ mm) is 11%, and the maximum for Case 7 ($l_t = 20$ mm) is 11%,

Next, the influence of the turbulent length scale, l_t, on the radiated noise is checked using the model of Amiet, [1]. In figure 6, these predictions are compared with the measurement data from [15]. Results are compared in a microphone placed 1 m above the leading edge of the wing, roughly in the main radiation direction. According to Amiet's model, an increase in l_t leads to a shift of the spectrum towards lower frequencies, and has a minor effect on the level. The agreement with measurement data is reasonable, but not sufficiently good to determine which l_t corresponds best to the experimental set-up. It is also noticeable that the measurement resolution for low frequencies is not sufficient to identify whether a peak exists in the spectrum. A further interesting uncertainty which concerns the model is how large the error is in the thin foil approximation. The assumption in the model is that of scattering from a plane (zero thickness) whereas the thickness of the NACA-0012 foil is comparable to the turbulent length scale. Furthermore, as was discussed for fluctuations in velocity components in connection with figures 3 and 5, the turbulence is significantly deformed at the leading edge. Hence, the inflow values (k, l_t) are hardly accurate at the sound source (the leading edge). These are well-known issues, see e.g. [4, 13], and various techniques exist to improve the models, such as

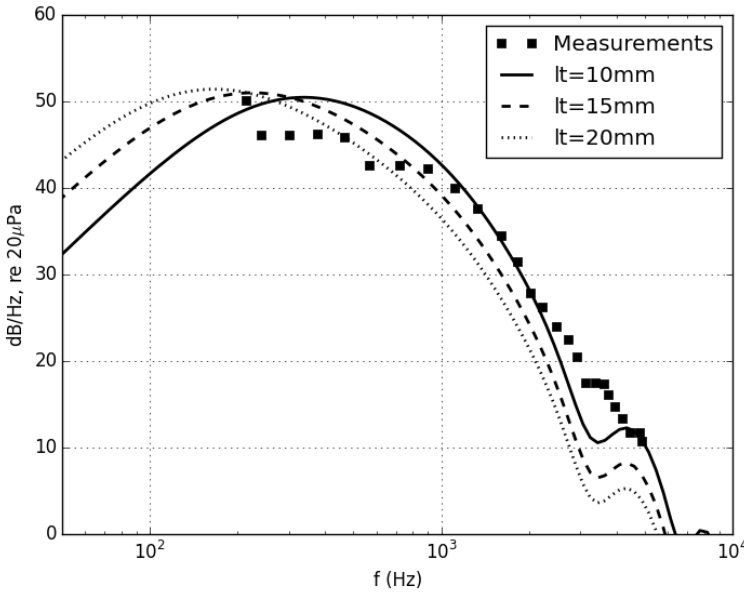

Figure 6. Sound-pressure spectrum in a microphone located 1 m above the wing leading edge, $(x,y,z) = (0,0,1)$ m. The curves indicate spectra obtained with Amiet's model, [1], with $k = 4.86\,\mathrm{m^2/s^2}$ and varying turbulence length scale, l_t, as indicated in the graph (10, 15 and 20 mm, respectively). The measurement data is from figure 14 in [15].

Rapid-distortion theory as applied in, [15]. It is however an area where LES-based predictions may provide a significant improvement over existing techniques due to the potential to accurately simulate the interaction of the inflow turbulence with the foil leading edge. At the time of writing of this paper however, the processing of the results from the acoustic analogy has not been fully carried out, but will be included in future publications.

4 CONCLUSIONS

Large-eddy simulation was applied to investigate a foil in strong inflow turbulence, corresponding to the experimental set-up of [15]. The influence of turbulence level and turbulent length scale was investigated in the simulation campaign. The turbulent length scale, 10–20 mm, is comparable to the thickness of the foil, 11.9 mm. The analysis was focused on the flow around the leading edge, and the deformation of the turbulence in this region, including comparison with measurements.

Significant modification of the level of fluctuations in the velocity components occurs only quite near to the leading edge, at a distance of less than 2 mm. Hence it is challenging to characterize it with measurements, and it is also believed that many RANS turbulence models have difficulties prediction the components of the Reynolds stress in this region. At the same time, these flow features are critical for the flow-generated sound at the leading edge.

The results in figure 5 show large discrepancies between the LES results and the measurements of [15]. In the author's opinion, the LES results are more accurate. This is supported by the unphysical behaviour of the measurement curve for $\sigma(u')$ which should decay to zero at the leading edge, and also by the fact that the grid resolution for LES should be sufficiently fine to accurately capture this part of the flow. This opinion should be substantiated by a mesh refinement study, which would provide error estimates for the LES prediction. It is noted that the measurements of this difficult flow quantity are not provided with uncertainty quantification in [15]. The simulation results show an increase in the fluctuation level of the upwash velocity component near

the leading edge as the turbulent length scale, l_t, is decreased. The fluctuation level of the other two velocity components is rather insensitive to l_t.

In conclusion, further work is necessary to clarify the exact behaviour of the turbulence near the leading edge. It is believed that LES is a tool which can provide accurate prediction of the relevant flow quantities. These can then be used either as input to simplified noise models of the type described in, [1, 13], or directly input into an acoustic analogy as described in section 2. At the time of writing of this paper, the processing of the results from the acoustic analogy has not not been fully carried out, but will be included in future publications.

5 ACKNOWLEDGEMENTS

Paul Croaker is gratefully acknowledged for interesting discussions and valuable insights concerning different modelling techniques for flow-generated sound. His assistance in producing the results of the acoustic model in figure 6 is also much appreciated.

REFERENCES

[1] R. K. Amiet. Acoustic radiation from an airfoil in a turbulent stream. *Journal of Sound and Vibration*, 41(4):407–420, 1975.

[2] W. K. Blake. *Mechanics of flow-induced sound and vibration*. Academic Press, 1986.

[3] N. Curle. The influence of solid boundaries upon aerodynamic sound. *Proc. R. Soc. Lond. A*, 231:505–514, 1955.

[4] W. J. Devenport, J. K. Staubs, and S. A. L. Glegg. Sound radiation from real airfoils in turbulence. *Journal of Sound and Vibration*, 329:3470–3483, 2010.

[5] P. D. Francescantonio. A new boundary integral formulation for the prediction of sound radiation. *Journal of Sound and Vibration*, 202(4):491–509, 1997.

[6] F. F. Grinstein, L. G. Margolin, and W. J. Rider, editors. *Implicit Large Eddy Simulation, Computing Turbulent Fluid Dynamics*. Cambridge University Press, 2007.

[7] N. Kornev and E. Hassel. Method of random spots for generation of synthetic inhomogeneous turbulent fields with prescribed autocorrelation functions. *Commun. Numer. Meth. Engng*, 25:35–43, 2007.

[8] M. Liefvendahl and R. E. Bensow. Simulation-based analysis of hull-propeller interaction for a single-screw transport ship. In *30th Symposium on Naval Hydrodynamics*, Hobart, Tasmania, Australia, 2014.

[9] M. Liefvendahl and R. E. Bensow. Simulation-based analysis of flow-generated noise from cylinders with different cross-sections. In *32nd Symposium on Naval Hydrodynamics*, Hamburg, Germany, 2018.

[10] T. Marić, J. Höpken, and K. Mooney. *The OpenFOAM Technology Primer*. sourceFlux, 2014.

[11] R. W. Paterson and R. K. Amiet. Acoustic radiation and surface pressure characteristics of an airfoil due to incident turbulence. Technical Report CR-2733, National Aeronautics and Space Administration, 1976.

[12] S. Rezaeiravesh, T. Mukha, and M. Liefvendahl. Systematic study of accuracy of wall-modeled large-eddy simulation using uncertainty quantification techniques. *Computers & Fluids*, 185:34–58, 2019.

[13] M. Roger and S. Moreau. Extensions and limitations of analytical airfoil broadband noise models. *International journal of aeroacoustics*, 9(3):273–305, 2010.

[14] P. Sagaut. *Large eddy simulation for incompressible flows.* Springer-Verlag, 2 edition, 2002.

[15] L. D. Santana, J. Christophe, C. Schram, and W. Desmet. A rapid distortion theory modified turbulence spectra for semi-analytical noise prediction. *Journal of Sound and Vibration*, 383:349–363, 2016.